

# Hollow Cathode and Keeper-Region Plasma Measurements Using Ultra-Fast Miniature Scanning Probes

Dan M. Goebel, Kristina K. Jameson, Ron M. Watkins, Ira Katz  
Jet Propulsion Laboratory, California Institute of Technology, Pasadena, CA 91109

In order to support the development of comprehensive performance and life models for future deep space missions that will utilize ion thrusters, we have undertaken a study of the plasma structure in hollow cathodes using a new pneumatic scanning probe diagnostic. This device is designed to insert a miniature probe directly into the hollow cathode orifice from either the upstream insert region in the interior of the hollow cathode, or from the downstream keeper-plasma region at the exit of the hollow cathode, to provide complete axial profiles of the discharge plasma parameters. Previous attempts to diagnose this region with probes was limited by the melting of small probes in the intense discharge near the orifice, or caused significant perturbation of the plasma by probes large enough to survive. Our new probe is extremely compact, and when configured as a single Langmuir probe, the ceramic tube insulator is only 0.5mm in diameter and the current collecting conductor has a total area of 0.002 cm<sup>2</sup>. A series of current-voltage characteristics are obtained by applying a rapid sawtooth voltage waveform to the probe as it is scanned by the pneumatic actuator into and out of the plasma region. The bellow-sealed pneumatic drive scans the probe 4 cm in the cathode insert region and 10 cm in the anode/keeper plasmas region at average speeds of about 1 mm/msec, and the residence time at the end of the insertion stroke in the densest part of the plasma near the orifice is measured to be only 10 msec. Since the voltage sweep time is fast compared to the motion of the probe, axial profiles of the plasma density, temperature and potential with reasonable spatial resolution are obtained. Measurements of the internal cathode pressures and the axial plasma-parameter profiles for a hollow cathode operating at discharge currents of up to 35 A in xenon will be presented.

## Nomenclature

$A$	= probe area
$e$	= electron charge
$I$	= probe current
$k$	= Boltzman's constant
$n$	= plasma density
$m$	= electron mass
$M$	= ion mass
$T_e$	= electron temperature
$V_p$	= probe potential
$\phi$	= plasma potential

## I. Introduction

Hollow cathodes represent one of the most critical technologies in modern electron-discharge ion thrusters, and yet appear to be the least well understood of all the components in the thruster. After nearly 40 years of investigation and decades of use in thrusters, there are no definitive models of the plasma density, temperature and potential distributions capable of describing different thermionic hollow cathode configurations and discharge conditions, and only limited empirical data of the geometry dependence on the life and performance. In order to provide data on the ion fluxes and energies to the surfaces exposed to the plasma discharge in the thruster, we have undertaken a probe study of the cathode, keeper and cathode-plume regions of a hollow cathode discharge. Fast scanning probes are used to produce on-axis profiles of the plasma density, potential and temperature for different

discharge currents and gas flow rates. This data, coupled with detailed modeling presented in other papers at this conference, provides a basic understanding of the hollow cathode physics and permits the determination of the sputtering of the cathode structures that ultimately determines the cathode life.

Probing of thermionic hollow cathodes has been performed since they were invented by Lidsky<sup>1</sup> in the 1962. Familiar thermionic hollow cathode geometries were described by Rawlings<sup>2</sup> for mercury thrusters, Moore<sup>3</sup> for cesium thrusters, and Sovey<sup>4</sup> for noble-gas magnetic-cusp thrusters. The definitive probe study of a mercury hollow cathode was performed by Siegfried and Wilbur<sup>5</sup> in 1978. In this study, moveable probes were placed in different positions in the insert region and in the keeper/plasma plume region of a mercury cathode operated without an applied axial magnetic field. Moving the probes to new positions in steps produced profiles of density, potential, and temperature. Since the probes were of significant size to avoid melting and were moved into position manually and were stationary during data acquisition, the region near the cathode orifice was unreachable and the discharge was limited to currents below about 10 A. However, densities in excess of  $1 \times 10^{14} \text{ cm}^{-3}$  were measured in the hollow cathode and axial profiles of these plasma parameters away from the cathode orifice for spot mode and plume modes operation were obtained. Hayakawa<sup>6</sup> published in 1989 probe data downstream from a hollow cathode in a 14 cm ring-cusp thruster, and found evidence of primary electrons in the distribution function. These experiments produced data within 1.6 cm of the cathode, but did not approach the keeper or cathode-orifice regions.

In the present work, single Langmuir probes have been sized as small as practical (0.5 mm diameter ceramics and 127  $\mu\text{m}$  diameter electrodes) to minimize any perturbation of the plasma in a xenon hollow cathode discharge. The miniature probes are scanned rapidly into and out of the orifice region from the upstream and downstream regions to avoid overheating of the probe. Rapid voltage sweeps applied to the probes provide complete axial profiles of density, temperature and plasma potential with a reasonable position resolution of typically 0.5 mm. Since the probes reside in the plasma for only a very short time, discharge currents of over 35 A have been used without damaging the probe. Plasma densities in the hollow cathode of over  $10^{14} \text{ cm}^{-3}$  at temperatures of 2 to 5 eV are observed, depending on the current and flow rate. It is found that the plasma potential on axis in the cathode is on the order of 10 to 15 V, and decreases as the discharge current increases at a given flow rate. The cathode plasma is very collisional, and the radial Bessels-function profile expected for this case drops roughly half this voltage in the plasma before the cathode sheath<sup>7,8</sup>. Surprisingly, the highest density is always found upstream of the orifice. Axial plasma potential discontinuities associated with double layers and/or highly resistive regions of the plasma are observed in most situations in the orifice and downstream of the keeper, although the location and magnitude of these layers depend strongly on the discharge conditions. The plasma outside the cathode falls from mid- $10^{13} \text{ cm}^{-3}$  in the orifice region to mid- $10^{11} \text{ cm}^{-3}$  5 to 10 cm from the cathode. Two anode geometries has been used to produce a variation in the discharge voltage, which impacts the potential profiles.

The accuracy of the probe data generally degrades as the experimental difficulty increases, and probing these plasmas is extremely difficult. The plasma density is found to vary several orders of magnitude between the cathode insert region, the orifice region and the rapidly diverging plume in the anode region. The probes are very small and moving fast to avoid melting in the orifice plasma, which requires high-speed bias circuits and data acquisition systems. Inside the cathode, the probe encounters plasma densities well in excess of  $10^{14} \text{ cm}^{-3}$  and random electron fluxes of over 1  $\text{kA/cm}^2$ , which causes probes tips with only  $2 \times 10^{-3} \text{ cm}^2$  of exposed area to collect over 2.5 A in the electron saturation region. Since the cathode probe resides inside the hollow tube upstream of the insert prior to the scan, it is heated by radiation to about 800°C and coated by backflowing barium, which makes the electrode easy to become an emissive probe if overheated by excessive time in the electron saturation regime during the scan. The anode probe is exposed to  $>10^{13} \text{ cm}^{-3}$  densities and up to 100 Gauss in the keeper/orifice region, and  $<5 \times 10^{11} \text{ cm}^{-3}$  densities and a few Gauss in the anode region, which traverses thin and thick sheath theory and unmagnetized and magnetized plasma theory for analysis of the probe data. Finally, the probes sample regions with strong potential and density gradients, which distort the electron distribution function and can produce finite plasma drift velocities. These effects combine to limit the accuracy of the data derived from the probe signals. Nevertheless, reproducible density, potential and temperature profiles with reasonable accuracy have been obtained that provide important information on how the hollow cathode works. The electron temperatures presented here are derived from fits to the probe data with fitting coefficients  $R^2 \geq 0.99$ , and have estimated errors of  $\pm 0.5$  eV. A sensitivity study of fitting to the electron saturation region of our probe traces indicates that the plasma potential error is less than  $\pm 1$  V in the cathode and  $\pm 2$  V in the anode region. The plasma density calculation is insensitive to the electron temperature due to the square root dependence, but is sensitive to the collecting area. While factors of two are generally quoted for plasma densities from probe data, we anticipate errors closer to 50%. This paper will present only a fraction of the data taken with one hollow cathode configuration, and future work will examine different cathode sizes and operating parameters in order to bench mark the plasma models over a significant operating space.

## II. Experimental Hardware

A schematic illustration of the hollow cathode, support assembly and cathode scanning probe is shown in Figure 1. The cathode in these experiments has a conventional configuration of a barium impregnated tungsten insert in a 1.5 cm dia. molybdenum tube with a tungsten orifice plate e-beam welded on the end. The cathode is heated by a standard sheathed heater, which is turned off during discharge operation. The graphite keeper electrode fully encloses the cathode, and the keeper orifice is about 1.7 times the diameter of the cathode orifice. The cathode and scanning probe system is mounted on an 8" Conflat flange installed a one port of 0.75-m diameter, 2-m long vacuum chamber. The chamber is pumped by two 10" CTI cryopumps with a combined xenon pumping speed of 1275 l/sec. The base pressure of the chamber is below  $1 \times 10^{-8}$  Torr, and during normal operation at less than 10 sccm of xenon flow the chamber pressure remains in the  $10^{-5}$  Torr range. The bellows isolated pneumatic plunger for the cathode probe (not shown) is mounted to the mini-conflat flange shown exterior to the chamber. The pneumatic drive shaft is coupled inside the vacuum chamber to a bellows mounted between an SMA feedthrough flange connected to the probe and a six-way mini-conflat cross. Actuation of the plunger moves the SMA flange on a linear slide, compresses the bellows and inserts the single Langmuir probe into the hollow cathode. The xenon gas is controlled and measured by a digital MKS mass flow controller and injected into the hollow cathode through one port on the six-way cross. Since the plunger action will change the pressure inside the hollow cathode by decreasing the volume of the enclosed system, a second bellows on another linear slide arrangement is mounted on one of the six-way-cross ports. This second bellows is coupled to the first such that compression of the primary bellows causes a proportional expansion of the second bellows to maintain a constant volume in the system. A third port on the six-way cross is connected to a precision Baratron capacitive manometer to measure the pressure in the hollow cathode during operation.

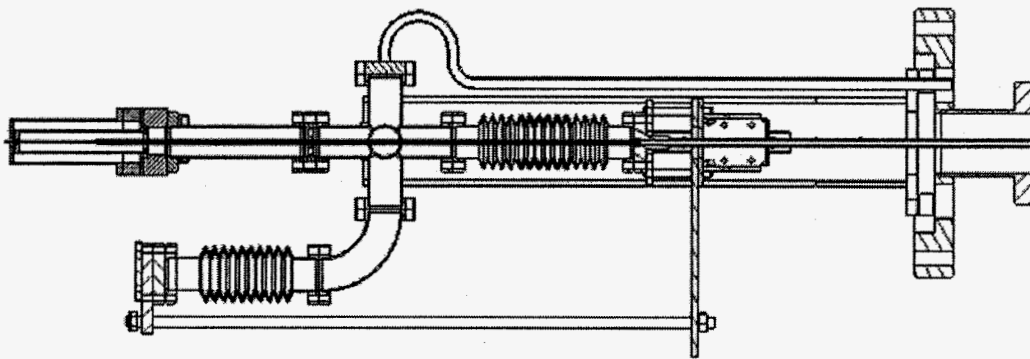


**Figure 1. Schematic drawing of the pneumatic scanning probe and dual bellows arrangement used to measure the pressure and plasma parameters in the hollow cathode.**

The cathode scanning probe assembly mounted in the vacuum system is shown in Figure 2. The original experimental arrangement used a water-cooled cylindrical anode that was 5 cm in diameter and about 12 cm long. The probe tip is 0.5mm diameter alumina tubing with a 0.127mm diameter tungsten wire electrode that sticks out of the small-bore ceramic tubing a distance of 0.5mm, as seen in Fig. 2b. Since the cross-sectional area of the 0.127mm dia. ceramic tube is  $0.2 \text{ mm}^2$  and the area of the 2.75mm dia. Cathode orifice used in these experiments is  $5.9 \text{ mm}^2$ , the probe occupies less than 3.5% of the orifice area and does not significantly perturb the plasma discharge. The probe is aligned axially in the system by two slide-guides internal to the cathode system and positioned downstream of the six-way vacuum cross. The slide guides are designed with a maximum transparency to gas to minimize any pressure drop so as to not introduce error in the cathode pressure measurements. When fully inserted, the probe extends through the cathode orifice plate to the exit plane of the keeper (not installed in Fig. 2). Also shown in Fig. 2 is a solenoid coil wound on a water cooled cylinder directly around the cathode to provide a diverging axial magnetic field of adjustable amplitude at the cathode exit that simulates the field in ring-cusp thrusters.

The anode scanning-probe is shown in Figure 3. The photograph on the left shows the pneumatic plunger and vacuum bellows arrangement mounted on the outside of the vacuum system. The photograph on the right shows the probe tip (without the cylindrical anode installed) approaching the keeper orifice, where the diameter of the ceramic tubing is stepped down from 3 mm to 0.5 mm diameter for the 3 cm section that is inserted deepest into the plasma in order to minimize perturbation to the plasma in the anode region. The exposed electrode is again a 0.127 mm

tungsten wire, but has a length of 1.3mm in order to collect sufficient current away from the keeper region to accurately determine the plasma parameters.

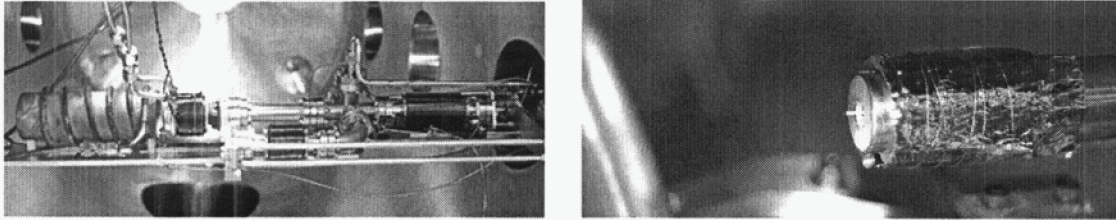


**Figure 2. Cathode scanning probe assembly with cylindrical anode mounted in the vacuum chamber, and the probe tip extending out of the cathode orifice with the keeper removed.**

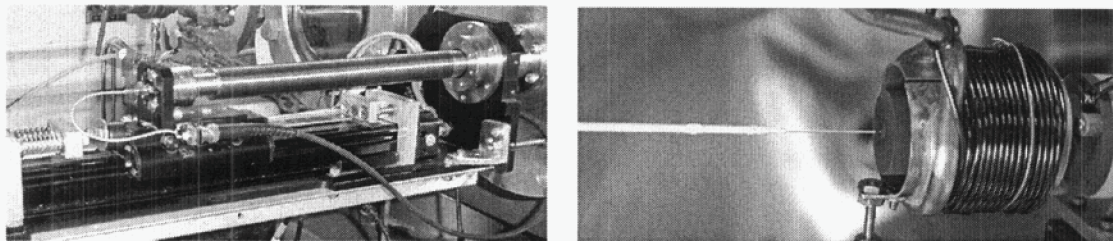


**Figure 3. Anode scanning probe assembly outside the vacuum system showing the high speed pneumatic plunger and bellows arrangement, and the probe tip approaching the keeper orifice.**

Experiments with the cylindrical anode demonstrated stable discharge currents of 5 to 35 A were possible at corresponding cathode flow rates in the range of 3 to 8 sccm. At the nominal discharge current from the current-controlled power supply of 25 A and the nominal flow rates from the regulated gas system of 5 sccm, the discharge voltage was found to be only about 16 V. Since typical thrusters operate in the neighborhood of 25 V, it was decided to modify the anode geometry to a conical shape similar to the rear of NSTAR-type thrusters to raise the discharge voltage. Figure 4 shows a schematic of the water-cooled, conical anode installed in the vacuum system with the two probe drives. The anode was constructed of six isolated segments so that the current distribution could be measured as a function of the total discharge current, flow rate and magnetic field strength.

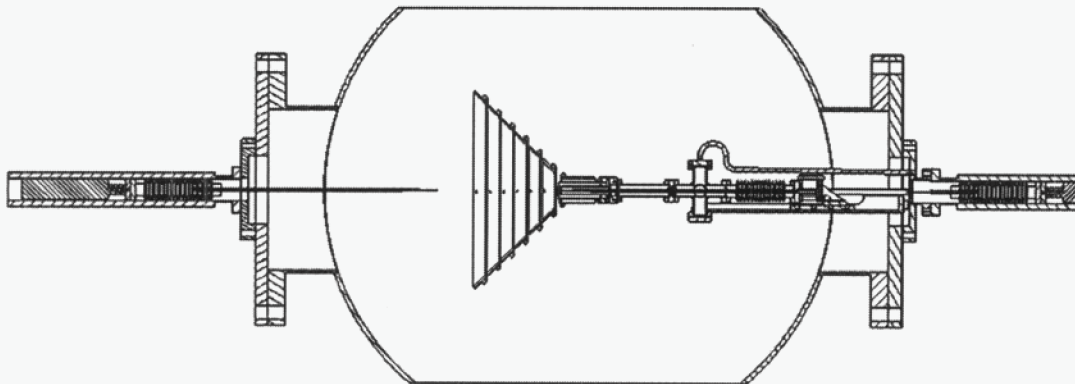


**Figure 4. Cut-away schematic of the two probe assemblies mounted on the vacuum chamber and the cathode with the conical, segmented anode.**

The probes are driven by high pressure (100 PSI of nitrogen), reciprocating pneumatic plungers. Precise control of the insertion and retraction valve timing determines the depth of insertion and the dwell time. A linear position transducer is mounted to each plunger (not shown), and this signal provides a measurement of the axial probe position with an uncertainty of 0.25 mm or less. Figure 5 shows the cathode and anode position as a function of time. The cathode probe is fully inserted in less than 40 msec, and has a dwell time in the orifice region of about

10 msec. The anode probe requires 80 msec to travel about 10 cm during insertion, and also has a dwell time of about 10 msec in the keeper plasma region. The radial alignment of the probes on axis is controlled by slide-guides internal to the cathode assembly, and by a slide-guide mounted inside the vacuum system about 20 cm from the flange for the anode probe assembly. The cathode probe radial alignment is very good because of the shorter stroke and dual guide arrangement, resulting in a radial offset of less than 0.25 mm. The anode probe has nearly three times the throw and 5 times the unsupported length so as to not perturb the anode-plasma. This causes a radial misalignment typically about 1 mm at the keeper electrode, although this can be reduced to about 0.5mm by very careful iterative alignment techniques. The anode probe can be fully inserted into the cathode orifice, although whip of the long ceramic sometimes causes the tip to touch the keeper or cathode during retraction. Figure 6 shows a photograph of the anode probe inserted through the segmented anode into the cathode spot in front of the keeper for a low current discharge case.

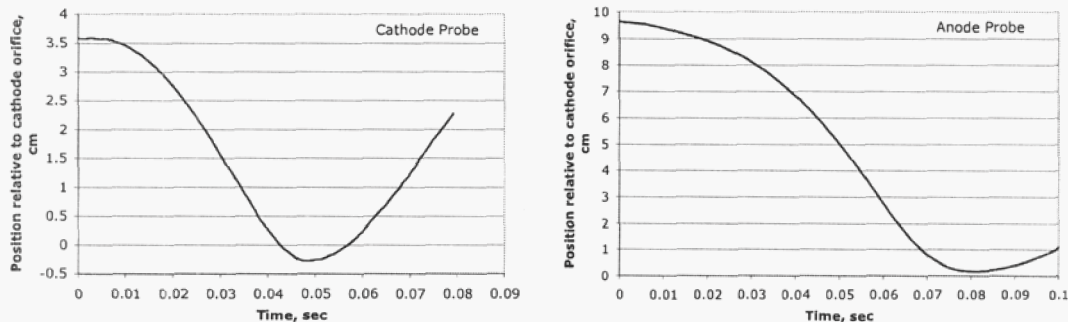


**Figure 5. Probe tip position relative to the cathode orifice plate upstream entrance versus time. The probes travel at an average speed of about 1mm/msec and dwell at the full insertion for about 10 msec.**

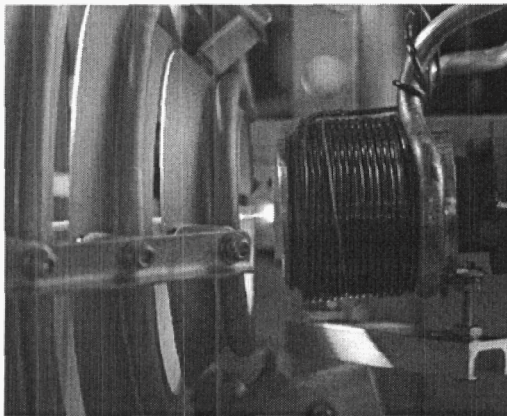


**Figure 6. Anode probe inserted through the segmented anode into the cathode spot emerging from the keeper electrode. Solenoid coil around the cathode is also seen.**

The bias voltage applied to the probe tip is generated by a programmable waveform synthesizer that drives a Kepco bipolar power supply. The voltage waveform is a sawtooth ramp that scans from  $-10$  to  $+50$  V in a time of 1 msec. The repetition rate of the voltage ramp is typically 1 kHz for the anode probe and 500 Hz for the cathode probe. The cathode probe is swept less often during the scan to avoid overheating the probe tip in the high-density plasma near the hollow cathode orifice. Since the probe are moving at 1mm/msec and the region of the Langmuir trace where the electron temperature and plasma potential are determined from is less than half of the total 1 msec trace, the position uncertainty for the plasma parameters is on the order of 0.5 mm over most of the scan and less than 0.025 mm near the full insertion point where the probe is stopping. The probe position, voltage and current data is collected on a PC at a sample rate of 275 kHz, resulting in 275 data points in each probe characteristic curve.

The influence of the probe insertion on the discharge has been carefully studied. We find that the discharge voltage and current are unchanged during the insertion of the cathode probe through the orifice plate and into the keeper orifice. The discharge voltage increases less than 1 V with the cathode probe fully inserted to the keeper orifice plate exit. After several milliseconds in this region, the discharge voltage starts to climb up to 2 V, and the discharge may start to show oscillations. For this reason, we acquire probe data only during the insertion period when the affect on the discharge is minimal.

Two typical Langmuir traces are shown in Figure 7 from the anode probe (a) near the keeper and the cathode probe (b) in the insert region. The upper graphs show the standard negative current versus bias voltage, and the lower graphs are semi-log plots showing the plasma potential and electron temperature from curve fits to the data. In regions where the characteristics are well represented by Figure 7, the electron temperature has a reasonable error of about 1 eV and plasma potential can be found within about 1 volt. However, the anode probe is found at distances

of over 2.5 cm from the cathode to be in the thick-sheath regime, and the ion and electron “saturation” regions have significant slope that must be accounted for with orbit theory<sup>9,10</sup> to determine the plasma density and potential. The probe curves also often demonstrate non-classical shapes in the regions where strong potential gradients are observed in the orifice and keeper regions, which causes significant rounding in the plasma potential region and slope in the electron and ion saturation regions associated with non-Maxwellian electron distributions. In these cases, the accuracy of the plasma potential determination degrades and the errors increase to  $\pm 1$  to 2 volts. The plasma density in the thin-sheath regime regions is calculated from scans with the probe biased to ion saturation, which doesn't depend on knowing the plasma potential and depends only on the square-root of the electron temperature. The error in the plasma density is certainly less than a factor of two in this situation.

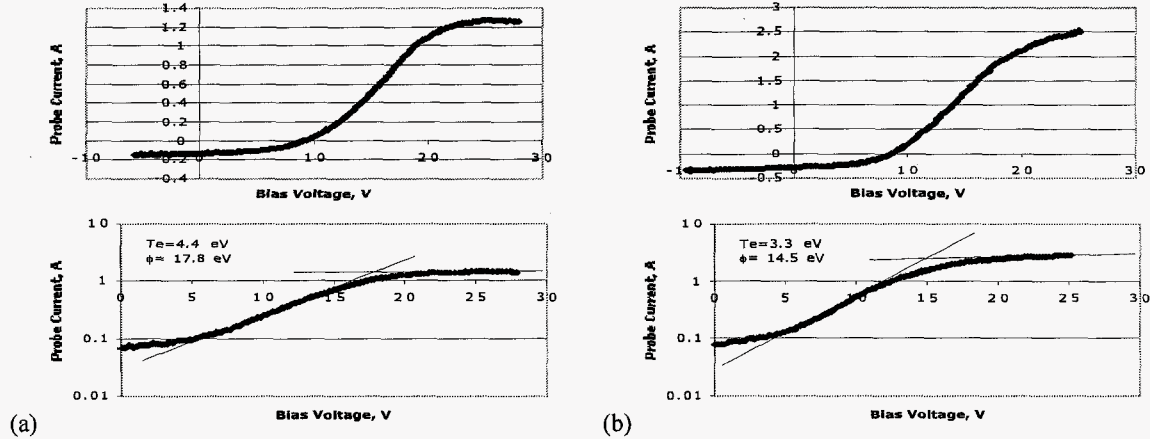


Figure 7. Typical Langmuir probe traces from the anode probe (a) near the keeper and the cathode probe (b) in the insert region. The upper graphs show the standard negative current versus bias voltage, and the lower graphs are semi-log plots showing the plasma potential and electron temperature.

### III. Experimental Results

The pressure inside the hollow cathode is measured by the Baratron manometer, and can also be accurately calculated by a 1-D variable-diameter disk model that accounts for the viscous and molecular conductance contributions along the cathode length and through the orifice. Figure 8(a) shows the pressure measured and calculated as a function of xenon gas flow for the cases of room temperature and heater only (no plasma). The agreement between the model and the measurement is excellent. The plasma discharge, however, heats the gas and increases the pressure inside the hollow cathode at a given flow and discharge current. Figure 8(b) shows the pressure measured at 5 sccm of gas flow as a function of the discharge current. The gas flow model was then used to predict the effective gas temperature required to produce the observed pressure with plasma, as shown in Fig. 8(b). At the nominal condition of 5 sccm, 25 A of discharge current and 2 A of keeper current, the effective gas temperature is found to be 2750 °C.

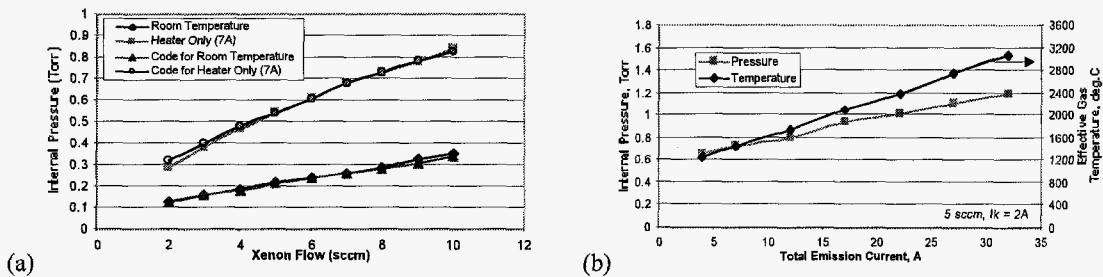


Figure 8. Pressure measured and calculated inside the hollow cathode without plasma (a), and with plasma (b) indicating significant gas heating by the plasma discharge.

The plasma density profile measured by both probes is shown in Figure 9 for the case of 25 A of discharge current and 5.5 sccm using the conical segmented anode. To obtain these profiles, the probes were biased negatively relative to the cathode into ion saturation, scanned through the system, and the current and position data collected by the computer. The plasma density in the thin sheath regime is evaluated from the Bohm current<sup>9,11</sup>:

$$I = \frac{1}{2} n e \sqrt{\frac{kT_e}{M}} A \quad (1)$$

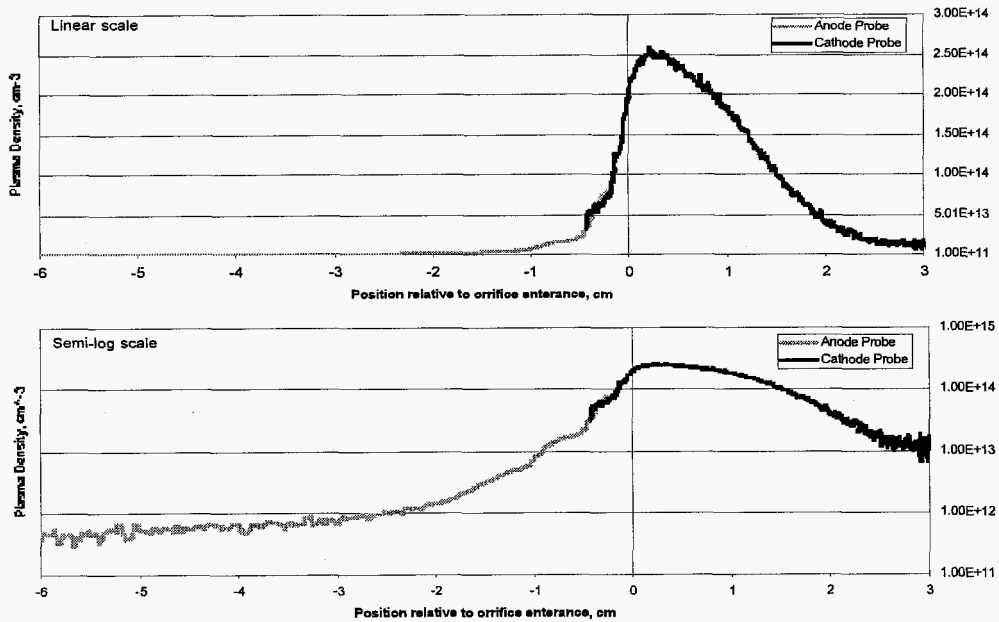


Figure 9. Axial plasma density profiles plotted on a linear scale (a) and a semi-log scale (b) for 25 A and 5.5 sccm.

The electron temperature used in Eq. 1 is obtained from the Langmuir probe data by fitting the exponential region of the current versus voltage curve in the standard manner<sup>9</sup>. The plasma density in the thick sheath regime (typically encountered 3 to 4 cm from the keeper for the small anode-probe used) is found from LaFramboise<sup>10</sup>. The electron temperature in the thick sheath regime is determined from Chen<sup>9</sup>, although this technique is found to be relatively crude and often gives largely varying and high electron temperatures. The appropriateness of the probe

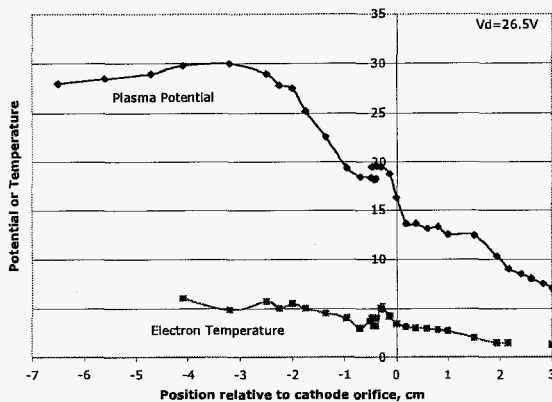


Figure 10. Plasma potential and temperature profiles for the 25 A, 5.5 sccm case.

theory used (thin or thick sheath) is checked periodically by calculating the ratio of the debye length to the probe radius<sup>9,10</sup> and comparing the slope of both "saturated" regions of the probe curves. If the regime is found to be questionable, either the other theory is used or the data is discarded. We have occasionally used large stationary flat probes in the far downstream region to check the cylindrical scanning probe results, and in the future plan to scan large probes through this region for better accuracy data.

The plasma potential and temperature profiles for the case of Fig. 9 are shown in Fig.10. In this experiment, the conical anode was used and the discharge ran at 26.8 V, 25 A for 5.5 sccm of cathode flow. The plasma potential inside the hollow cathode on axis is found to be about 13

eV. It should be pointed out again that this is not the cathode sheath voltage due to the radial potential drop in the very collisional cathode plasma. In the orifice, the potential jumps to nearly 20 eV. The anode probe for this scan measured a plasma potential of about 18 V, which is slightly lower than the cathode probe due to radial misalignment of the probe estimated to be on the order of 1 mm. A more careful alignment estimated to be within 0.5 mm found agreement between the probes within one volt, which is essentially the accuracy of the plasma potential determination by probe methods in any case. Although there appears to be a double layer in the orifice region, the potential change is normally in the 5 to 10 eV range and the plasma potential in the orifice and keeper region is found not to be the highest in the system, as suggested by some authors<sup>12</sup> for high current hollow cathodes. However, this potential profile may be due to a relatively low current density in the large-orifice hollow cathode used in these experiments, which is less than 600 A/cm<sup>2</sup> at discharge currents up to 35 A. The potential distribution observed in our cathode slowly increases to a maximum of about 30 V several cm downstream of the keeper. This is due to both the structure of the cathode plume and the increasing electron temperature observed as the probe moves downstream. The peak potential is about 3.2 V higher than the anode potential, and the plasma potential then falls downstream of the peak as the plasma density decreases further. Electron temperatures on the order of 2 to 3 eV are found inside the cathode insert and 4 to 6 eV are measured in the anode region.

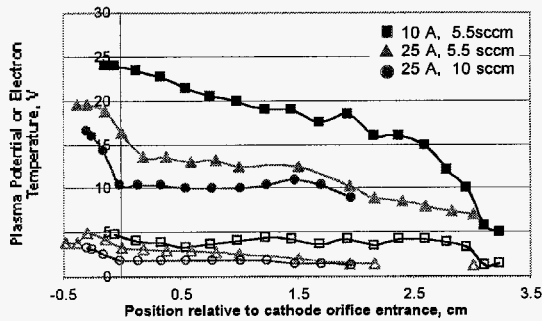


Figure 11. Plasma potential and electron temperature in the hollow cathode showing variation with flow and discharge current.

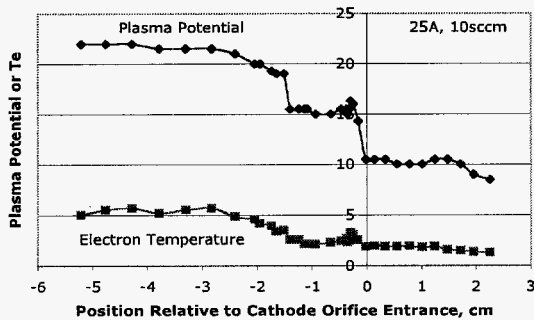


Figure 12. Plasma potential and electron temperature profiles from the 25A, 10 sccm case.

layer in the orifice plate is clearly seen, another potential discontinuity is observed downstream about 1 cm from the keeper exit. This is consistent with visual observations of the cathode “spot” shape and location. Figure 13 shows of the visible emission from the 25 A, conical anode tests, where the upper photo shows the cathode plume at 5.5 sccm and the lower photo shows the plume at 10 sccm. The cathode “spot” moves significantly downstream at the high flow rates and a dark space is clearly observed. The dark space corresponds to a region of low electron temperature where excitation is decreased. However, this reduced-luminosity region also is observed in the 5.5 sccm case, although it is closer to the keeper and less apparent in the photograph. The downstream potential step

Increasing the gas flow rate at a fixed discharge current always decreases the discharge voltage and the electron temperature measured throughout the system. The plasma potential change with flow rate depends on the discharge current level. At 25 A, the plasma potential inside the hollow cathode on axis is observed to decrease as the flow is raised from 5.5 to 10 sccm, as shown in Fig. 11. However, at 10 A and 5.5 sccm, the potential on axis is over 20 V and the electron temperature exceeds 4 eV. It is clear that the cathode adjusts the potential at a given discharge current to provide adequate self heating. At lower discharge currents, higher potential drops are required to produce the required cathode temperature to supply the electron emission required to support the discharge current set by the current controlled power supply. This higher potential drop in the cathode plasma also tends to produce higher electron temperatures. The potential in the orifice region is observed to follow any discharge voltage changes, although it is not a linear response due to changes in the potential distributions outside the cathode. In Figure 11, the data was taken with the conical anode and the discharge voltage was 29 V for the 10 A case, 26.8 V for the 25 A, 5.5 sccm case, and 20.5 V for the 25 A, 10 sccm case. Higher flow rates at a given current also tend to push the observed double layer further downstream in the orifice. It is likely that smaller orifice diameters will also push the double layer downstream at the same flow rate due to the higher neutral density in the insert and orifice region.

The potential distribution in the anode region also changes with flow rate. Figure 12 shows the complete plasma potential and electron temperatures profiles for the 25 A, 10 sccm case. While the characteristic double

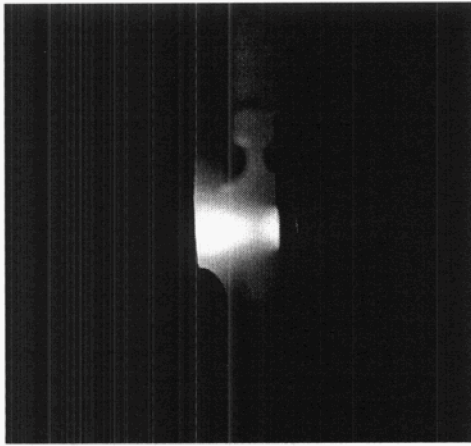
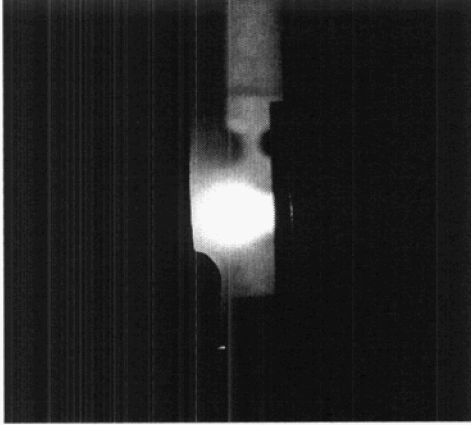


Figure 13. Cathode spot for 25 A discharge for 5.5 sccm (top) and 10 sccm (bottom).

shown in the 10 sccm case in Fig. 12 actually occurs at the downstream edge of the spot (or ball). This behavior is predicted by a model developed by Katz<sup>7</sup> that finds insufficient plasma generation and heating in this region to carry the discharge current without a double layer.

Interestingly, the 5.5 sccm case has a distinct visual boundary on the downstream edge of the cathode spot, seen at the left of Fig. 13a, but the probe data indicates that this does not correspond to a double layer as in the 10 sccm situation. In the lower flow cases, the strong axial density gradient measured in this region creates the visual impression of a distinct boundary (the “ball” or “spot” shape) where the probe data says that no potential or temperature step is observed.

#### IV. Discussion

Single probes provide a reasonably good indication of the temperature of the bulk of the Maxwellian-electron distribution, but can be insensitive to distortions of the distribution at higher temperatures or energies. A qualitative indication of this effect can be obtained from the floating potential. Figure 14 shows the floating potential of a probe scan inside the cathode and relative to the cathode potential for our nominal 25 A, 5.5 sccm case. We see that the floating potential jumps sharply in the orifice region where the double layer is found, and also falls below zero upstream of the insert. In the bulk of the cathode plasma, the floating potential is about 2.2 eV. Assuming the electron distribution is a pure Maxwellian, the floating potential can be found by equating the ion current to the probe given by

$$I_e = \frac{1}{4} ne \sqrt{\frac{8kT_e}{\pi m}} A \exp\left[\frac{e(V_p - \phi)}{kT_e}\right], \quad (2)$$

where the floating potential relative to the plasma potential is  $V_p = (V_p - \phi)$ . Solving for the floating potential (relative to the plasma potential) gives

$$V_f = \frac{kT_e}{e} \ln\left[\frac{\pi m}{2M}\right]^{1/2}, \quad (3)$$

For xenon, the floating potential from Eq. 3 is  $5.97T_e$  negative relative to the plasma. From Fig.11, the plasma potential in the peak region in the insert for this case is about 13 eV and the electron temperature is 3 eV. From Eq. 3, we would expect the floating potential to be 17.9 V below the plasma potential, which would be -4.9 V relative to the cathode potential. This is clearly inconsistent with the data of Fig. 14 where the floating potential is +2.2 V relative to cathode potential. If Eq. 3 is correct, the electron temperature would have to be 1.8 eV. This discrepancy can easily be explained by a depletion of the tail of the electron distribution function. Since the first ionization and excitation energies for xenon are both just above 10 eV, we might expect that the highly collisional plasma in the cathode insert region could deplete the tail above 10 eV. This tail-

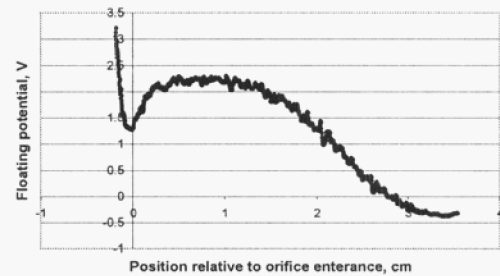
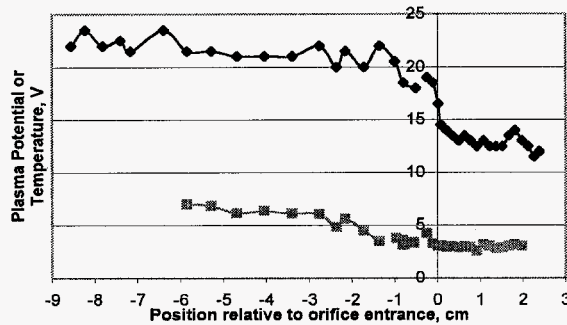


Figure 14. Cathode probe floating potential versus position.

depletion effect has been directly observed in other xenon plasmas<sup>13</sup> where the collision mean free paths are significantly shorter than the plasma dimensions. Since the floating potential is very sensitive to the high-energy electron content, a depleted tail will result in more positive floating potentials consistent with the data in the cathode plasma. A non-Maxwellian electron distribution function complicates the cathode modeling considerably.



**Figure 15. Plasma potential and electron temperature for the nominal 25A case with the cylindrical anode. The potential in the orifice region transitions rapidly to the anode plasma potential, which is essentially uniform on axis along the length of the anode tube.**

anode potential, and is relatively flat over the scan range. The conical anode also showed 3 to 4 V plasma potentials above the anode voltage, but the discharge required higher voltages to generate the anode plasma and conduct the current the anode. This is likely because the gas density is significantly lower in the anode region in the conical anode case. This implies that larger thrusters with anodes significantly away from the cathode will probably require higher cathode flow rates to operate at the same discharge voltages as small thrusters.

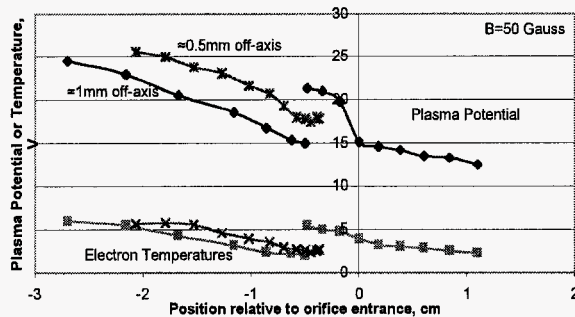


**Figure 16. Plasma potential and electron temperature for the nominal 25A case with 50 G applied magnetic field. The smaller plume size near the keeper makes the anode probe misalignment more critical.**

appears to be more peaked on axis in the magnetic field case, and small misalignments of the anode probe result in a significant mis-match in the data. In this case, the probe was re-aligned after the initial data to be near the minimum radial error, and the anode-probe potential was found to approach better the cathode probe data. It is clear that radial probe data will have to be taken in the axial field case to fully understand the profiles.

Finally, the hollow cathode showed clear indications of both long-term and short-term conditioning. When first turned on, the discharge voltage was observed to decrease slowly over several hundred hours and then stabilize. If exposed to air for any significant time, the discharge voltage at a given flow would increase 2 to 3 V, and then require on the order of 10 hours to fully recover. The probe data showed that the plasma potential inside the insert region tracked the discharge voltage. This is consistent with the work function depending on conditioning and on the history of the cathode surface. Environmental effects that might raise the work function are handled in the "self-

In these experiments, the shape of the anode electrode strongly affected the discharge voltage. The original cylindrical anode produced typically 16 to 17 V discharges at the nominal 25 A and 5.5 sccm. Installing the conical anode geometry raised the anode voltage to 25 to 26 V, and produced the potential profiles previously shown in Fig. 10. The potential and temperature profiles in the cylindrical anode case at 25 A and 5.5 sccm are shown in Fig. 15. We see that the plasma potential in the cathode insert and orifice regions is essentially unchanged. Modification of the anode geometry did not affect the basic cathode operation because these potentials and temperatures are sufficient to deliver the desired discharge current at the given cathode flow rate. The anode geometry changes modify only the potential exterior to the cathode in the anode-plasma region. The plasma potential in the cylindrical anode region is about 4 V positive relative to the

Applying an axial magnet field is observed to change the plasma characteristics considerably. The plasma density increases by a factor of typically 1.5 to 2 throughout the probed region, and the plasma appears visually much brighter. Figure 16 shows the plasma potential and electron temperature in the vicinity of the orifice plate for our nominal case of 25 A and 5.5 sccm, but with 50 Gauss (at the orifice) of applied magnetic field from the coil. The discharge voltage for this case increased about 2 V from the nominal to 29 V. Application of a magnetic field affects the plasma potential even inside the cathode where the plasma is very collisional. Compared to the no-applied field case, the peak plasma potential inside the cathode increases 1 to 2 V and the potential in the orifice/keeper regions increases by about the same amount. However, the cathode plume plasma

heating” system by the plasma increasing the power delivered to the cathode, which increases the temperature to sufficient levels to produce the required electron emission. The higher plasma potential inside the cathode raises the sheath voltage and ion bombardment energy, and the resistive drop radially also heats the plasma which delivers additional energy to the surface from tail-electrons overcoming the retarding sheath. This conditioning and history dependence is being studied further at this time to determine its impact on the life and reliability of hollow cathodes used in ion thrusters.

## V. Conclusion

Probe studies of hollow cathode discharges have provided considerable insight into the plasma potential, density and temperature structure though the system. Fast scanning probes are extremely useful in obtaining this data in regions of the discharge too intense for slow or stationary probes. This work has demonstrated the potential structure in hollow cathode discharges varies significantly with time, discharge current, flow rate, anode geometry and cathode geometry. The ion energy and fluxes bombarding the different surfaces are impacted by all these effects, and modeling of these parameters will continue to need data such as this for benchmarking. Since the data presented is here only for a single hollow cathode geometry, future work will also expand the parameter and geometry space to help construct a comprehensive model of the hollow cathode discharge. Of additional interest is the lack of evidence for very high energy primary electrons in the discharge and for large potential hills near the cathode exit that could produce the primaries or high energy ions observed in some hollow cathode discharges. It has been suggested that these effects may have been reduced or eliminated by the relative low current density in the large orifice used in these experiments. Future experiments on smaller cathodes and different discharge conditions will examine these effects.

## References

- <sup>1</sup>Lidsky, L., Rothleder, J. Rose, D., Yoshikawa, S., Michelson, C., Mackin, r., J. Appl. Phys. **22** (1962) p.2490.
- <sup>2</sup>Rawlings, V., Pawlik, E., “A Mercury Plasma Bridge Neutralizer”, *J. Spacecraft Rockets*, **5** (1968) p.814.
- <sup>3</sup>Moore, R. “Magneto-Electrostatically Contained Plasma Ion Thruster”, AIAA Paper #69-260, 7<sup>th</sup> Electric Propulsion Conference, Williamsburg, VA, March 3-5, 1969.
- <sup>4</sup>Sovey, J. “Performance of a Magnetic Multipole Line-Cusp Argon Ion Thruster”, AIAA Paper #81-0745, AIAA Electric Propulsion Conference, Las Vegas, Nevada, April 21-23, 1981.
- <sup>5</sup>Siegfried, D. and Wilbur, P., “An Investigation of Mercury Hollow Cathode Phenomena”, AIAA Paper #78-705, 13<sup>th</sup> International Electric Propulsion Conference, San Diego, CA, April 25-27, 1978.
- <sup>6</sup>Hayakawa, Y., Miyazaki, K., Kitamura, S., “Measurements of Electron Energy Distributions in a 14 cm Diameter Ring-Cusp Ion Thruster”, AIAA Paper #89-2715, 25<sup>th</sup> Joint Propulsion Conference, Monterey, CA July 10-12, 1989.
- <sup>7</sup>Katz, I., Mikellides, I., Goebel, D., “Model of the Plasma Potential Distribution in the Plume of a Hollow Cathode”. AIAA Paper #2004-4108, 40<sup>th</sup> Joint Propulsion Conference, Ft. Lauderdale, FL, July 11-14, 2004.
- <sup>8</sup>Mikellides, I., Katz, I., Goebel, D., Polk, J., “Model of a Hollow Cathode Insert Plasma”, AIAA Paper #2004-3817, 40<sup>th</sup> Joint Propulsion Conference, Ft. Lauderdale, FL, July 11-14, 2004.
- <sup>9</sup>Chen, F. “Electric Probes”, in *Plasma Diagnostics Techniques* (ed. R. Huddelstone and S. Leonard), Academic Press, NY (1966) p. 113-200.
- <sup>10</sup>Laframboise, J., UTIAS Report #100, University of Toronto, 1966.
- <sup>11</sup>Bohm, D., *The Characteristics of Electrical Discharges in Magnetic Fields*, edited by A. Gutrie and R.K. Wakerling (McGraw-Hill, New York, 1949) Chap.3.
- <sup>12</sup>Kameyama, I. Wilbur, P., “Potential Hill Model of High Energy Ion Production near High Current Hollow Cathodes”, ISTS Paper #98-a-2-17, 21<sup>st</sup> International Symposium on Space Technology and Science, Sonic City, Omiya, Japan, May 24-21, 1998.
- <sup>12</sup>Schwabedissen, A., Benck, E., Roberts, J., “Langmuir Probe Measurements in an Inductively Coupled Plasma Source”, *Phys. Rev. E*, **55**, (1997) p. 3450-3459.